Neoclassical tearing mode control using electron cyclotron current drive and magnetic island evolution in JT-60U

A. Isayama, G. Matsunaga, T. Kobayashi, S. Moriyama, N. Oyama, Y. Sakamoto, T. Suzuki, H. Urano, N. Hayashi, Y. Kamada, T. Ozeki, Y. Hirano, L. Urso[1], H. Zohm[1], M. Maraschek[1], J. Hobirk[1], K. Nagasaki[2] and the JT-60 team

Japan Atomic Energy Agency, Naka, Ibaraki 311–0193, Japan

[1] Max-Planck-Institut für Plasmaphysik, EURATOM Association, D–85748 Garching, Germany

[2] Institute of Advanced Energy, Kyoto University, Uji, Kyoto 611–0011, Japan

Abstract. The results of stabilizing neoclassical tearing modes (NTMs) with electron cyclotron current drive (ECCD) in JT-60U are described with the emphasis on the effectiveness of the stabilization. The range of the minimum EC wave power needed for complete stabilization of an $m/n = 2/1$ NTM was experimentally identified for two regimes using unmodulated ECCD to clarify the NTM behaviors with different plasma parameters: $0.2 < j_{\rm EC}/j_{\rm BS} < 0.4$ for $W_{\rm sat}/d_{\rm EC} \sim 3$ and $W_{\rm sat}/W_{\rm marg} \sim 2$, and $0.35 < j_{\rm EC}/j_{\rm BS} < 0.46$ for $W_{\rm sat}/d_{\rm EC} \sim 1.5$ and $W_{\rm sat}/W_{\rm marg} \sim 2$. Here, m and n are the poloidal and toroidal mode numbers; $j_{\rm EC}$ and $j_{\rm BS}$ the EC-driven current density and bootstrap current density at the mode rational surface; $W_{\rm sat}$, $W_{\rm marg}$ and $d_{\rm EC}$ the full island width at saturation, marginal island width and full width at the half maximum of the ECCD deposition profile, respectively. Stabilization of a 2/1

NTM using modulated ECCD synchronized with a mode rotation of about 5 kHz was performed, in which it was found that the stabilization effect degrades when the phase of the modulation deviates from that of the ECCD at the island O-point. The decay time of magnetic perturbation amplitude due to the ECCD increases by 50% with a phase shift of $\pm 50^\circ$ from the O-point ECCD, thus revealing the importance of the phasing of modulated ECCD. For near X-point ECCD, the NTM amplitude increases, revealing a destabilization effect. It was also found that modulated ECCD at the island O-point has a stronger stabilization effect than unmodulated ECCD by a factor of more than 2.

PACS number: 52.35.Py, 52.55.Tn, 52.55.Wq, 52.55.Fa

1. Introduction

To sustain a high-beta plasma with positive magnetic shear, such as that in the Inductive and Hybrid operations in ITER [1], controlling neoclassical tearing modes (NTMs) is essential since they degrade plasma performance and sometimes cause disruption. NTMs with the poloidal mode number $m = 2$ and toroidal mode number $n = 1$ in particular need to be suppressed as they can seriously affect the plasma: as shown later, the degradation of the beta value is typically 30–50% in JT-60U experiments.

Two NTM suppression scenarios have been developed in JT-60U, the first being NTM avoidance where the onset of NTM is avoided by optimizing the current and pressure profiles. In previous JT-60U experiments, the long-duration sustainment of a high-beta plasma was demonstrated [2, 3]. Although this scenario has the advantage of only requiring neutral beams (NBs), the optimization is not necessarily consistent with other factors such as the current drive. Similar demonstrations of stationary sustainment of high-performance plasmas have been also performed in other devices such as ASDEX-U, DIII-D and JET [4–6]. Cross-machine comparisons toward the development of the ITER Hybrid Scenario have also been performed [7].

The second scenario for NTM suppression is active stabilization using localized current drive. NTM stabilization using electron cyclotron (EC) wave is considered to be the most promising due to the ability of highly localized current drive. Experiments on the stabilization of $m/n = 3/2$ and $2/1$ NTMs using electron cyclotron current drive (ECCD) have been performed in JT-60U since the first gyrotron was installed in 1999, with several new stabilization techniques being demonstrated such as stabilization through the real-time steering of the EC mirror [8] and *preemptive* stabilization [9].

In addition, simulation of an NTM evolution using TOPICS-IB code has been also performed [10–12], and island evolution reproduced by determining the undetermined coefficients using experimental data. Stabilization of an NTM using ECCD has been also performed in ASDEX-U and DIII-D. In both devices, m/n=3/2 and 2/1 NTMs have been successfully stabilized. In ASDEX-U, a 3/2 NTM was completely stabilized by modulating the EC wave in synchronization with the NTM rotation [13]. In DIII-D, the onset of a 2/1 NTM was suppressed to the no-wall beta limit through real-time equilibrium reconstruction and optimizing the ECCD location with a change in the toroidal field or plasma position [14]. However, detailed research on effective stabilization of an $m/n = 2/1$ NTM, such as what the minimum required EC wave power is for complete stabilization and whether modulated ECCD is actually superior to unmodulated ECCD, remained as future work. Since this is an important issue also in ITER, experimental demonstration and verification is considered to be valuable.

This paper describes the results of active control of an $m/n = 2/1$ NTM using localized ECCD at the mode location in JT-60U. In Section 2, the results of identifying the minimum EC wave power necessary to completely stabilize a 2/1 NTM is described. In the experiments, the range of the minimum power in two regimes with toroidal magnetic fields of 3.7 T and 1.7 T was determined. In Section 3, the results of NTM stabilization using modulated ECCD is described. EC wave power was modulated in synchronization with the mode rotation frequency ($\sim$ 5 kHz). The effect of the phase difference between magnetic perturbations and modulated EC wave power was then investigated, and a comparison with unmodulated ECCD also made. A summary of this paper is then described in Section 4.

2. Minimum EC Wave Power for Complete Stabilization

As mentioned in the previous section, NTM stabilization using ECCD has been extensively preformed in JT-60U. However, as in other devices, the NTMs were *overstabilized* in most cases, and the EC wave power was larger than the minimum required power. Although NTMs should be stabilized with less EC wave power in ITER, it remains uncertain how much EC wave power is required as the minimum, thus making identification of the minimum required EC wave power an important issue. To clarify the minimum required power, stabilization of an $m/n = 2/1$ NTM with reduced EC wave power was performed.

Experiments were performed in two regimes of the different toroidal fields at 3.7 T and 1.7 T, which will be referred to as Case 1 and Case 2, respectively. The typical discharge in the high field (Case 1) is shown in figure 1, where plasma current $I_{\rm p} = 1.5$ MA, toroidal field $B_{\rm t} = 3.7$ T and safety factor at 95% flux surface $q_{95} = 4.1$, major radius $R = 3.18$ m, minor radius $a = 0.80$ m, triangularity at the separatrix $\delta = 0.20$. The toroidal field was fixed in time throughout this and all other discharges. In the series of discharges, neutral beams of about 25 MW were injected and the normalized beta $\beta_{\rm N}$ increased to about 2. An NTM with $m/n = 2/1$ appeared at $t \sim 5.7$ s, and the value of $\beta_{\rm N}$ decreased to about 1.4. Since the mode locked soon after onset, the behavior is unclear in the frequency spectrum shown in figure 1(c). At $t = 7$ s, the NB power was decreased and the direction of the tangential NBs changed from balanced injection to counter injection to raise the mode frequency. The 2/1 NTM started to rotate in the counter direction at $t = 7.5$ s, and the mode frequency became almost constant at about 4–5 kHz, as shown in figure 1(c). Fundamental O-mode EC waves with a frequency of

110 GHz were injected at $t = 9.5$ s by up to 3 gyrotrons. Changing the power and combination of the gyrotrons enables a variety of injection powers. The direction of the ECCD is the same as the plasma current, i.e. co-direction in all discharges in this paper. The injection angle of the EC wave, i.e. ECCD location, was fixed throughout the ECCD for all discharges after the optimum injection angle was determined. The temporal evolution of the structure of the magnetic island measured with an electron cyclotron emission (ECE) radiometer with a channel separation of about 2 cm, which corresponds to $\sim$0.02 in the volume-averaged normalized minor radius (ρ), is shown in figure 1(d). Here, $\rho = r_{\rm v}/a_{\rm v}$ with $r_{\rm v} = \sqrt{V/2\pi^2 R}$, $a_{\rm v}$ being the volume-averaged plasma minor radius and V the plasma volume inside the flux surface. The two bright peaks correspond to the separatrix of the island while the dark region between the two peaks corresponds to the center of the island. In this discharge, the major radius was shifted inward by 4 cm at $t = 8.0$–8.5 s. The change in the island location due to this shift can be clearly seen in the contour plot. As shown in this figure, the center position of the magnetic island remained unchanged during the ECCD, with the shot-to-shot difference of the island center being less than the channel separation of the ECE radiometer. This type of high-resolution measurement was important in the experiments because the stabilization effect strongly depends on the ECCD location. The mode location, $\rho_{\rm s}$, was about 0.6, and the full island width before ECCD, $W_{\rm sat}$, 0.12 (The normalized value using the volume-averaged plasma minor radius.). After the ECCD, the distance between the two peaks shown in figure 1(d), which corresponds to the full island width, decreased, and the 2/1 NTM was completely stabilized at $t = 12.0$ s. An ELMy H-mode plasma was sustained during the NB phase.

Similar experiments were carried out in lower field (Case 2) with the second harmonic X-mode ECCD, as shown in figure 2. The typical plasma parameters were as follows: $I_{\rm p} = 0.85$ MA, $B_{\rm t} = 1.7$ T, $R = 3.38$ m, $a = 0.88$ m, $q_{95} = 3.5$ and $\delta = 0.37$, with the discharge scenario being similar to that in the Case 1. An $m/n = 2/1$ NTM was first destabilized with NBs of about 20 MW, and after the mode onset the power was stepped down to about 9 MW. The value of $\beta_{\rm N}$ and the mode frequency were kept almost constant at 1.5 and 2–3 kHz, respectively. The values of $\rho_{\rm s}$ and $W_{\rm sat}$ just before ECCD were ~ 0.7 and 0.15, respectively. In this discharge, the 2/1 NTM was completely stabilized at $t \sim 9$ s.

The plasma configurations of the two discharge regimes are shown in figures 3(a) and 3(b). The cold resonance surfaces of a 110 GHz EC wave with the fundamental O-mode and the second harmonic X-mode were located at 3.02 and 2.95 m, respectively. By injecting the EC wave nearly tangentially to the flux surface, a narrow ECCD deposition width was obtained because the width of the absorption layer extended by the Doppler shift along the ray path (typically ~ 20 cm) can be reduced in the ρ space. The poloidal injection angles for Cases 1 and 2 were 16° and 13°, respectively (Angle defined as the depression angles). The toroidal injection angle was $\sim 22°$ in both configurations. The profile and amount of EC-driven current were calculated using EC-Hamamatsu code [15], in which the ray trajectory of the EC wave is calculated by the ray-tracing method, and the EC-driven current is calculated by the relativistic Fokker-Planck equation. The full-width at half maximum (FWHM) of the ECCD deposition width, $d_{\rm EC}$, was 0.08 with Case 1 and 0.05 with Case 2.

Figure 4 shows the temporal evolution of the magnetic perturbation amplitude, $\tilde{B}$,

near the minimum EC wave power for complete stabilization. With Case 1, while the 2/1 mode was completely stabilized for EC wave power $P_{\mathrm{EC}} = 1.3$ MW, it was not completely stabilized for $P_{\mathrm{EC}} = 1.0$ MW. And hence the minimum EC wave power was located between 1.0 and 1.3 MW in this experiment. With Case 2, the stabilization effect weakened with decreasing EC wave power, and complete stabilization was not achieved for $P_{\mathrm{EC}} = 0.3$ MW, thus revealing that the minimum EC wave power was located between 0.3 and 0.5 MW.

Both experimental regimes had similar island evolutions: the island first quickly decayed, then slowed down, and finally quickly decayed again. This behavior is consistent with the description provided by the modified Rutherford equation, and was also observed in previous NTM experiments [12]. The width at which the final rapid decay begins is referred to as the marginal island width (hereinafter the full width of the marginal island width will be referred to as W_{marg}). In figure 4, the $\tilde{B}$ reaching the marginal island width corresponds to ~ 0.6 in Case 1 and ~ 0.9 in Case 2, respectively corresponding to $W_{\mathrm{marg}} = 0.06$ and 0.08. The marginal island width can also be roughly estimated by stepping down the NB power and investigating the beta value at which the NTM spontaneous decays. With Cases 1 and 2, the marginal β_{N} value, $\beta_{\mathrm{N}}^{\mathrm{marg}}$, was 0.4 and 0.8, respectively. And assuming the island width to be proportional to the beta value, which is a reasonable assumption for the NTM, the result is roughly consistent with the result of the above marginal island width.

The ratio of EC-driven current density (j_{EC}) to bootstrap current density (j_{BS}) at the mode rational surface is an important parameter to evaluate the efficiency of the NTM stabilization. In addition, the ECCD deposition width with respect to the

marginal island width is another important parameter because the EC-driven current inside the island O-point decreases as the NTM is stabilized if the ECCD deposition width is comparable or wider than the marginal island width, which is the case with most of the experimental conditions in JT-60U and also ITER. According to the results of ACCOME [16] and EC-Hamamatsu code calculations, the range of the threshold value is $0.35 < j_{\mathrm{EC}}/j_{\mathrm{BS}} < 0.46$ for Case 1 and $0.2 < j_{\mathrm{EC}}/j_{\mathrm{BS}} < 0.4$ for Case 2. Here, in the ACCOME code, the bootstrap current is calculated based on the Hirshman-Sigmar model [17]. Also, in this paper, the difference in the harmonics of the EC wave is considered only in the calculation of the EC-driven current. In previous JT-60U experiments, an $m/n = 2/1$ NTM was completely stabilized at $j_{\mathrm{EC}}/j_{\mathrm{BS}} = 0.5$ with fundamental O-mode ECCD, however, the minimum value of the required EC-driven current could not be identified [12]. The previous results proved consistent with the above new results. The parameters in the two regimes are summarized in Table 1, where the misalignment of the ECCD location, $\Delta\rho_{\mathrm{mis}}$, is also shown.

3. Stabilization of 2/1 NTM by Modulated ECCD

Stabilizing NTMs using modulated ECCD is thought to be more effective than with unmodulated ECCD. Stabilizing an $m/n = 3/2$ NTM experimentally using modulated second harmonic X-mode EC wave was previously performed in ASDEX-U [13,18]. Since adding the ability to modulate the EC wave power at several kHz significantly changes the design of gyrotrons, it is important to stabilize the more dangerous 2/1 NTM and clarify whether the modulated ECCD is actually more effective and if so by how much. In addition, issues in performing the modulated ECCD need clarifying in order to make

the NTM stabilization in ITER more reliable.

In JT-60U experiments, power modulation at several tens of Hz had been done to investigate heat wave propagation since the initial phase of first gyrotron operation [19]. Although the modulation frequency was increased every year, it was still rather low for NTM stabilization experiments, where a modulation frequency of about 5 kHz is required. In 2008, the high-voltage circuits of gyrotrons was modified to achieve the higher modulation frequency of up to $\sim$ 7 kHz [20, 21]. Magnetic probe signals are sent to the gyrotron control system to monitor NTM rotation. The magnetic probe is located 13.5° below the horizontal midplane and 87° from the EC antenna in the toroidal direction. The toroidal angle between the magnetic probe and the intersection of the EC ray trajectory and the cold resonance surface is about 80°.

In the experiments, the mode frequency as well as the mode location stayed almost constant in the steady state phase ($t \sim 9$ s with this discharge condition; refer to figure 1). However, in general, mode frequency changes over time. To synchronize the modulated EC wave with the NTM, a system of generating the trigger signal for power modulation using the magnetic perturbation signal was newly developed, where mode frequency is monitored in real time and the trigger signal generated in accordance [21]. Effectiveness was experimentally demonstrated and is shown in figure 5, and where the plasma configuration and discharge scenario are the same as in figure 1. In this discharge the mode frequency was changed from 4.3 to 6.1 kHz during ECCD. As can be seen in figure 5, the trigger signal was successfully generated in synchronization with the magnetic perturbations. Note that in the modulation system the trigger signal is generated taking the delay time of the actual power down from trigger into account. In

this discharge the 2/1 NTM was completely stabilized at $t = 10.4$ s.

The phase difference between a modulated EC wave and the magnetic perturbation signal is an important parameter for modulated ECCD. The stabilization effect reaches maximum when the phase difference corresponds to the O-point ECCD, and the stabilization effect weakens even becoming negative (i.e. destabilization), as the phase difference increases. And although numerical models can be used to calculate the stabilization effect, experimental verification is essential to validate the model and make better predictions of NTM stabilization in ITER. In investigating the phase effect on NTM stabilization, the phase of the modulated EC wave power with respect to magnetic perturbation was scanned. Figure 6 shows the temporal evolution of magnetic perturbation amplitude for phase differences of 0°, 90° and 180°. Note that the value of the phase difference is simply defined as the phase difference between raw signals. The injected power of the EC waves from gyrotrons #3 and #2 was 0.6 MW each. The power was modulated from 0–100% for #3 and 20–100% for #2 with respect to peak power. The duty cycle of the modulated ECCD was 50%, that is, 50% on-time and 50% off-time, as shown in the figure. The stabilization effect was observed during ECCD in the 0° case, with the magnetic perturbation amplitude increasing after turnoff of EC wave injection. No clear ECCD effect was observed in the 90° case. As shown in the expanded waveforms of the magnetic perturbation and EC wave power, the modulation phase was shifted as expected. With the 180° case the magnetic perturbation amplitude slightly increased, and then decreased after turnoff of EC wave injection, showing a destabilization effect.

Figure 7 shows the dependence of initial decay time, τ_{decay}, on the phase difference

around 0°. τ_{decay} was obtained by fitting the magnetic perturbation amplitude to the exponential function of $\exp(-t/\tau_{\mathrm{decay}})$ using the initial 300 ms data from the start of modulation in order to see the ECCD effect alone. As shown in the figure, the decay time reached a minimum at about $-10°$, which can be assumed to be O-point ECCD. The offset of the minimum phase difference can be roughly explained by the difference in the toroidal and poloidal angles between location of the ECCD and the magnetic probe. The curve is nearly symmetrical with respect to the minimum point. The results shown in figure 7 reveals that the phase error from O-point ECCD needs to be small to obtain a better stabilization effect. For example, to lower the degradation of the decay time to less than 50%, the phase error needs to be less than $\pm 50°$.

For unmodulated ECCD with the same peak power, the decay time was about 4 s, which is about 3 times longer than that for O-point ECCD, thus revealing the superiority of modulated ECCD at (or near) the island O-point. A similar example revealing the superiority of O-point ECCD is shown in figure 8. In this discharge, modulated ECCD of 0.6 MW with one gyrotron was followed by unmodulated ECCD of 1 MW with two gyrotrons. The phase difference of the modulated ECCD was about $-65°$. Decay time for the modulated ECCD and unmodulated ECCD was 1.9 s and 1.5 s, respectively. As shown in the figure, the mode amplitude during ECCD was similar, even with rather large phase error and smaller EC wave power, revealing the stronger stabilization effect of modulated ECCD.

As a theoretical model the stabilization efficiency can be described by integrating the current profile on the island flux surface [22–24]. Efficiency η_{EC} is defined as follows:

$$\eta_{\mathrm{EC}} = \int_{-1}^{\infty} \bar{j}_{\mathrm{EC}}(\Omega)\frac{R(\Omega)}{S(\Omega)}\mathrm{d}\Omega \Big/ \int_{-1}^{\infty} \bar{j}_{\mathrm{EC}}(\Omega)\mathrm{d}\Omega, \tag{1}$$

$$R = \oint \frac{\cos\alpha \mathrm{d}\alpha}{\sqrt{\Omega + \cos\alpha}}, \quad (2)$$

$$S = \oint \frac{\mathrm{d}\alpha}{\sqrt{\Omega + \cos\alpha}}, \quad (3)$$

where $\bar{j}_{\mathrm{EC}}$ is the flux surface average of EC-driven current, and the profile is assumed to be a Gaussian in real space. In these equations, $\alpha = 0^\circ$ and $\pm 180^\circ$ correspond to the O-point and the X-point of the magnetic island, and $\Omega = -1$ and 1 correspond to the center and separatrix of the island, respectively. The island structure and ECCD deposition profile are schematically shown in figure 9. In the calculations, values for the full island width, FWHM of ECCD deposition width and misalignment were set at 0.12, 0.08 and 0.02 in ρ, based on those in the JT-60U experiments. The duty ratio of the modulation was set at 50%. And although the EC-driven current is turned on and off without any time delay in this model, it is not always a good assumption with high modulation frequency in particular [24], thus, making experimental comparison important. The value of $1/\eta_{\mathrm{EC}}$ is equivalent to the above-defined decay time. Figure 10 plots $1/\eta_{\mathrm{EC}}$ as a function of the center phase of modulation α_{c}. As shown in this figure, $1/\eta_{\mathrm{EC}}$ increases as it deviates from the O-point ECCD, that is, the stabilization effect decreases. The criteria for the 50% degradation corresponds to a phase error of about 60°, which is similar to the above experimental observations.

Discussing the technical issues met in performing the modulated ECCD experiments could prove useful. As shown above, the EC wave was modulated with reference to the magnetic perturbation signal because in JT-60U the signal-to-noise ratio of the magnetic perturbation signal is better than the ECE signal. In some of the NTM experiments, instability other than the $m/n = 2/1$ mode was observed, such as the 3/2 mode. In addition, the plasma is usually in ELMy H-mode. An example in an NTM

experiment is shown in figure 11. ELM crash occurs at $t = 10.1935$ s [figure 11(a)], and at the same time a sharp pulse corresponding to the ELM crash is observed in the magnetic perturbation signal [figure 11(b)]. A trigger signal synchronized with the 2/1 NTM is not successfully generated by the ELM crash, as shown in figure 11(c). Further expansion of the magnetic perturbation signals is shown in figure 11(d), with the two major components of the signal with frequencies of 4.9 and 11.9 kHz, which correspond to 2/1 and 3/2 NTMs, respectively, being shown in figure 11(e). As shown in figure 11(a), even in this situation the trigger signal was generated as expected since the amplitude of the 2/1 mode dominated the signal. Although the 3/2 mode was much smaller than the 2/1 mode at the saturation phase, it cannot be considered negligible as the 2/1 mode was stabilized by ECCD. In this situation the trigger signal may not have been generated in synchronization with the 2/1 NTM. In addition sharp pulses due to the ELM could have affected the magnetic probe signal. Perturbation caused by the ELM was rather insignificant in the JT-60U NTM experiments because the 2/1 mode frequency ($\sim$ 5 kHz) was much higher than the ELM frequency (several tens of Hz). However, this kind of ELM effect may not be so insignificant in higher power regimes where higher ELM frequencies can be expected. And hence for future experiments, the development of a pre-processing scheme for the magnetic probe signals will be important.

4. Summary

The effect of localized ECCD on an $m/n = 2/1$ NTM has been performed with the emphasis on the effectiveness of the stabilization in JT-60U. In this paper, two topics which are important issues in ITER too have been described: minimum EC wave power

for complete stabilization and stabilization with modulated ECCD.

The range of the minimum EC wave power was investigated at $B_t = 3.7$ T and 1.7 T using fundamental O-mode ECCD and second harmonic X-mode ECCD, respectively. In the former case the minimum EC-driven current was located at $j_{EC}/j_{BS} = 0.35$–0.46 with $W_{sat} = 0.12$, $W_{marg} = 0.06$ and $d_{EC} = 0.08$. In the latter case the minimum EC-driven current was located at $j_{EC}/j_{BS} = 0.2$–0.4 with $W_{sat} = 0.15$, $W_{marg} = 0.08$ and $d_{EC} = 0.05$. In the experiments the gyrotron power was adjusted to make uncertainty in the threshold power as small as possible. Although the uncertainty was 0.2–0.3 MW, it is not small from the viewpoint of identifying the threshold power. Simulation using the TOPICS-IB code will complement that uncertainty. Detailed comparison remains as future work. In addition, comparison with other devices is important to extrapolate to ITER. The value of $j_{EC}/j_{BS} \sim 2.8$ required to suppress an $m/n = 2/1$ NTM has been previously reported [25]. Although parameters other than j_{EC}/j_{BS}, such as W_{marg}, d_{EC}, affect the threshold value, it has yet to have been clarified what exactly causes the difference. Cross-machine comparisons in the future will contribute to deeper understanding of the physics of the threshold value.

Stabilization using modulated ECCD in synchronization with magnetic perturbations was successfully performed. In the 2007–8 campaign, significant progress was made in the JT-60U EC wave system. First, the ability to modulate injection power was increased to ∼7 kHz by modifying the high-voltage circuits of gyrotrons to realize fast power downs [20]. Second, a new system to synchronize the modulated EC wave with NTM rotation was developed, in which the phase of the modulated EC wave is adjusted in real time [21]. Using the EC wave system, phase scans were then successfully

performed, and the effect of the phase shift of the modulated EC wave on stabilization was investigated in detail, which is shown in figures 6 and 7. The result showed that the stabilization effect weakens as the phase of the modulation deviates from that corresponding to O-point ECCD: τ_{decay} increases by $\sim 50\%$ with a phase shift of $\sim \pm 50^{\circ}$. It was also demonstrated that modulated ECCD actually has a stronger effect on NTM stabilization. The decay time for modulated O-point ECCD is less than 1/3 of that for unmodulated ECCD. The superiority of modulated ECCD was also demonstrated by comparing the stabilization effect for modulated ECCD with that for unmodulated ECCD. Although the phase error was rather large, $\sim -65^{\circ}$, similar decay of the magnetic perturbation amplitude was observed, even with $\sim 40\%$ smaller EC wave power (figure 8). In addition to the stabilization effect, a destabilization effect was observed with ECCD near the island X-point for the first time. Since a 2/1 NTM causes mode locking if the destabilization is large, phasing is important. Comparison with a theoretical model on ECCD efficiency was also made. It was found that the dependence of the decay time on phase shift with respect to O-point ECCD is similar to that of the inverse of the ECCD efficiency function. Similar experiments on $m/n = 3/2$ NTM stabilization in ASDEX-U showed that the decrease of magnetic island width by about 30%, which is comparable to that for unmodulated ECCD, was observed even with X-point ECCD [13]. Cross-machine comparisons will clarify the stabilization effect of modulated ECCD in more detail and allow better predictions for ITER NTM stabilization.

Acknowledgements

This work was partially supported by a Grant-in-Aid for Young Scientists (B) from MEXT Japan.

References

[1] Shimada M., Campbell D.J., Mukhovatov V., Fujiwara M., Kirneva N., Lackner K., Nagami M., Pustovitov V.D., Uckan N., Wesley J., Asakura N., Costley A.E., Donné A.J.H., Doyle E.J., Fasoli A., Gormezano C., Gribov Y., Gruber O., Hender T.C., Houlberg W., Ide S., Kamada Y., Leonard A., Lipschultz B., Loarte A., Miyamoto K., , Mukhovatov V., Osborne T.H., Polevoi A. and Sips A.C.C. 2007 *Nucl. Fusion* **47** S1

[2] Isayama A. and the JT-60 Team 2005 *Phys. Plasmas* **12** 056117

[3] Oyama N., Isayama A., Suzuki T., Koide Y., Takenaga H., Ide S., Nakano T., Asakura N., Kubo H., Takechi M., Sakamoto Y., Kamada Y., Urano H., Yoshida M., Tsuzuki K., Matsunaga G., Gormezano C. and the JT-60 Team 2007 *Nucl. Fusion* **47** 689

[4] Sips A.C.C., Tardini G., Forest C.B., Gruber O., McCarthy P.J., Gude A., Horton L.D., Igochine V., Kardaun O., Maggi C.F., Maraschek M., Mertens V., Neu R., Peeters A.G., Pereverzev G.V., Stäbler A., Stober J., Suttrop W. and the ASDEX Upgrade Team 2007 *Nucl. Fusion* **47** 1485

[5] Petty C.C., West W.P., DeBoo J.C., Doyle E.J., Evans T.E., Fenstermacher M.E., Groth M., Ferron J.R., McKee G.R., Politzer P.A., Schmitz L., Allen S.L., Austin M.E., Brooks N.H., Casper T.A., Chu M.S., Greenfield C.M., Holcomb C.T., Hyatt A.W., Jackson G.L., Kinsey J.E., La Haye R.J., Luce T.C., Makowski M.A., Moyer R.A., Murakami M., Osborne T.H., Rhodes T.L., Wade M.R., and Wang G. 2008 *Fusion Energy 2008 (Proc. 22nd IAEA Fusion Energy Conf., Geneva (IAEA, Vienna))* IAEA-CN-165/EX/1-4Rb, http://www-pub.iaea.org/MTCD/Meetings/FEC2008/ex_1-4rb.pdf

[6] Joffrin E., Hobirk J., Brix M., Buratti P., Buttery R.J., Challis C.D., Crisanti F., Giroud C., Gryaznevich M., Hender T.C., Imbeaux F., Koslowski R., Luce T., Mantica P., McDonald D. C.,

Pinches S.D., Saarelma S., Sips A.C.C., Villone F., Voitsekovitch I. and Zimmermann O. 2008 *Fusion Energy 2008 (Proc. 22nd IAEA Fusion Energy Conf., Geneva (IAEA, Vienna))* IAEA-CN-165/EX/1-4Ra, http://www-pub.iaea.org/MTCD/Meetings/FEC2008/ex_1-4ra.pdf

[7] Sips A.C.C., Casper T.A., Doyle E.J., Giruzzi G., Gribov Y., Hobirk J., Hogeweij G.M.D., Horton L., Hubbard A., Hutchinson I., Ide S., Isayama A., Imbeaux F., Jackson G.L., Kamada Y., Kessel C., Kochl F., Lomas P., Litaudon X., Luce T.C., Marmar E., Mattei M., Nunes I., Oyama N., Parail V., Portone A., Saibene G., Sartori R., Suzuki T., Tardini G., Wolfe S., the C-Mod team, the AUG team, the DIII-D team and JET EFDA contributors 2008 *Fusion Energy 2008 (Proc. 22nd IAEA Fusion Energy Conf., Geneva (IAEA, Vienna))* IAEA-CN-165/IT/2-2, http://www-pub.iaea.org/MTCD/Meetings/FEC2008/it_2-2.pdf; submitted to *Nucl. Fusion*

[8] Isayama A., Kamada Y., Hayashi N., Suzuki T., Oikawa T., Fujita T., Fukuda T., Ide S., Takenaga H., Ushigusa K., Ozeki T., Ikeda Y., Umeda N., Yamada H., Isobe M., Narushima Y., Ikeda K., Sakakibara S., Yamazaki K., Nagasaki K. and the JT-60 Team 2003 *Nucl. Fusion* **43** 1272

[9] Nagasaki K., Isayama A., Ide S. and JT-60 Team 2003 *Nucl. Fusion* **43** L7

[10] Hayashi N., Isayama A., Nagasaki K. and Ozeki T. 2004 *J. Plasma Fusion Res.* **80** 605

[11] Nagasaki K., Isayama A., Hayashi N., Ozeki T., Takechi M., Oyama N., Ide S., Yamamoto S. and the JT-60 Team 2005 *Nucl. Fusion* **45** 1608

[12] Isayama A., Oyama N., Urano H., Suzuki T., Takechi M., Hayashi N., Nagasaki K., Kamada Y., Ide S., Ozeki T. and the JT-60 team 2007 *Nucl. Fusion* **47** 773

[13] Maraschek M., Gantenbein G., Yu Q., Zohm H., Günter S., Leuterer F., Manini A., ECRH Group and ASDEX Upgrade Team 2007 *Phys. Rev. Lett.* **98** 025005

[14] Prater R., La Haye R.J., Luce T.C., Petty C.C., Strait E.J., Ferron J.R., Humphreys D.A., Isayama A., Lohr J., Nagasaki K., Politzer P.A., Wade M.R. and Welander A.S. 2007 *Nucl. Fusion* **47** 371

[15] Hamamatsu K. and Fukuyama A. 2001 *Fusion Eng. Design* **53** 53

[16] Tani K., Azumi M. and Devoto R.S. 1992 *J. Comp. Phys* **98** 332

[17] Hirshman S.P. and Sigmar D.J. 1981 *Nucl. Fusion* **21** 1079

[18] Zohm H., Gantenbein G., Giruzzi G., Günter S., Leuterer F., Maraschek M., Meskat J., Peeters A.G., Suttrop W., Wagner D., Zabiégo M., ASDEX Upgrade Team and ECRH Group 1999 *Nucl. Fusion* **39** 577

[19] Ikeda Y., Kasugai A., Takahashi K., Kajiwara K., Isayama A., Ide S., Terakado M., Shinozaki S., Yokokura K., Anno K., Shimono M., Hiranai S., Haga K., Kajiyama A., Ikeda Yu., Moriyama S., Tsuneoka M., Sakamoto K., Hamamatsu K., Oikawa T., Kamada Y., Naito O., Seki M., Ushigusa K., Imai T., Yamamoto T., Fujii T. and JT-60 Team 2001 *Fusion Eng. Design* **53** 351

[20] Moriyama S., Kobayashi T., Isayama A., Terakado M., Sawahata M., Suzuki S., Yokokura K., Shimono M., Hasegawa K., Hiranai S., Igarashi K., Sato F., Suzuki T., Wada K., Shinozaki S., Seki M., Kasugai A., Takahashi K., Kajiwara K., Sakamoto K. and Fujii T. 2008 *Fusion Energy 2008 (Proc. 22nd IAEA Fusion Energy Conf., Geneva (IAEA, Vienna))* IAEA-CN-165/FT/P2-26, http://www-pub.iaea.org/MTCD/Meetings/FEC2008/ft_p2-26.pdf; submitted to *Nucl. Fusion*

[21] Kobayashi T., Terakado M., Sato F., Yokokura K., Shimono M., Hasegawa K., Sawahata M., Suzuki S., Hiranai S., Igarashi K., Wada K., Suzuki T., Kajiwara K., Kasugai A., Sakamoto K., Isayama A., Matsunaga G. and Moriyama S. 2008 "Developments of High Power Gyrotron and Power Modulation Technique on JT-60U ECRF System"; submitted to *Plasma Fusion Res.*

[22] Hegna C.C. and Callen J.D. 1997 *Phys. Plasmas* **4** 2940

[23] Perkins F.W., Harvey R.W., Makowski M. and Rosenbluth M.N. Proc 24th European Physical Society Conference on Controlled Fusion and Plasma Physics (Berchtesgaden, 1997), Part III, p 1017

[24] Giruzzi G., Zabiégo M., Gianakon T.A., Garbet X., Cardinali A. and Bernabei S. 1999 *Nucl. Fusion* **39** 107

[25] Petty C.C., La Haye R.J., Luce T.C., Humphreys D.A., Hyatt A.W., Lohr J., Prater R., Strait E.J. and Wade M.R. 2004 *Nucl. Fusion* **44** 243

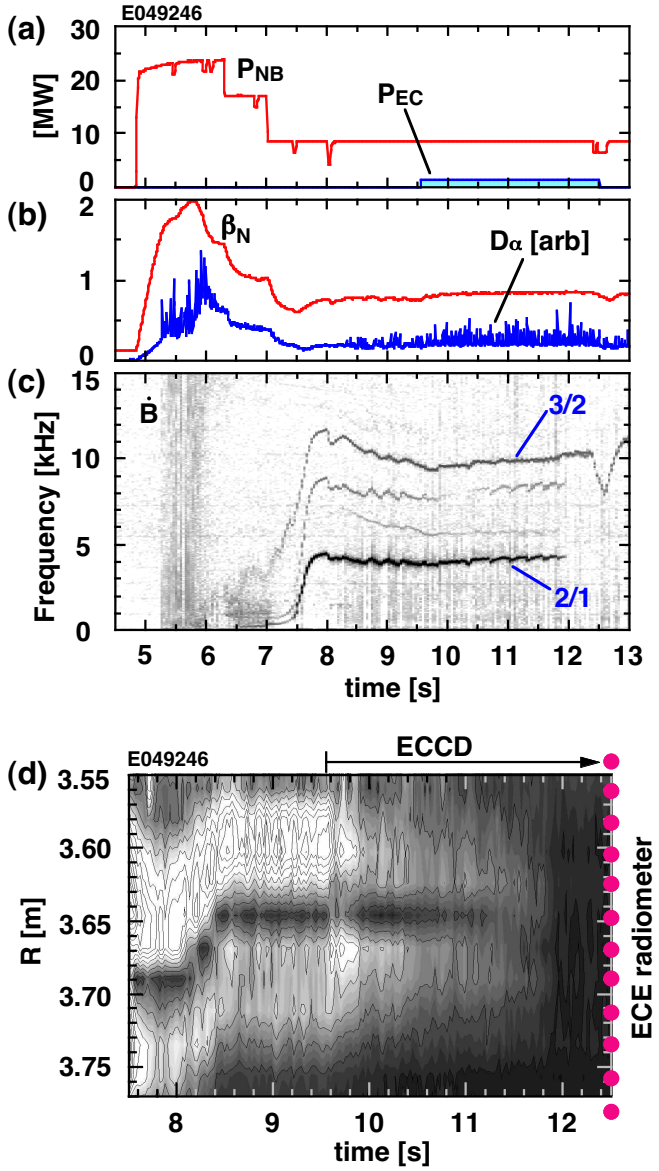

Figure 1. Typical discharge of 2/1 NTM stabilization with ECCD for Case 1: (a) injection power of NB ($P_{\rm NB}$) and EC wave ($P_{\rm EC}$), (b) Normalized beta ($\beta_{\rm N}$) and intensity of D_α line, (c) frequency spectrum of magnetic perturbation, and (d) contour plot of electron temperature perturbations. At $t = 9.5$ s. the island center is located at $R \sim 3.65$ m ($\rho \sim 0.6$).

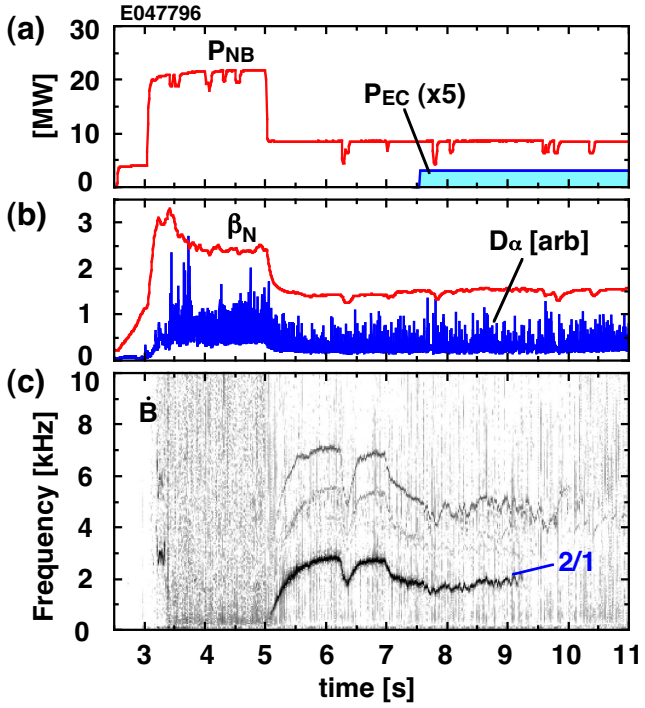

Figure 2. Typical discharge of 2/1 NTM stabilization with ECCD for Case 2: (a) injection power of NB (P_{NB}) and EC wave (P_{EC}), (b) Normalized beta (β_{N}) and intensity of D_{α} line and (c) frequency spectrum of magnetic perturbation.

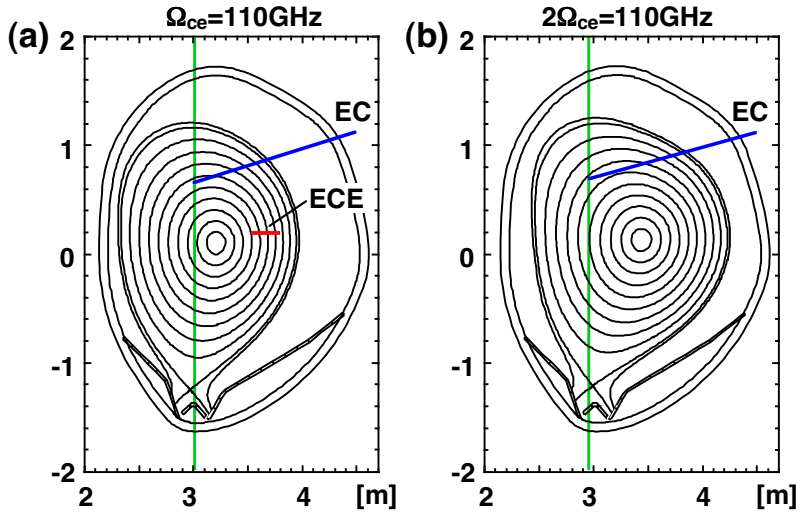

Figure 3. Plasma cross section, ray trajectory of EC wave and cold resonance layer for (a) Case 1 ($B_{\rm t}$=3.7 T) and (b) Case 2 ($B_{\rm t}$=1.7 T). Contour is drawn every 0.1 in ρ.

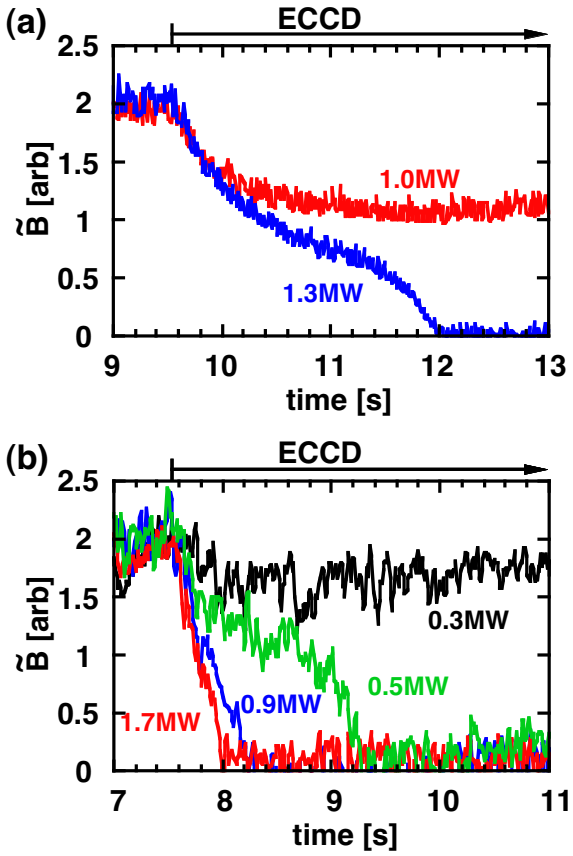

Figure 4. Temporal evolution of magnetic perturbation amplitude near the threshold EC wave power for (a) Case 1 and (b) Case 2.

	Case 1	Case 2
$I_{\rm p}$ [MA]/$B_{\rm t}$ [T]	1.5 / 3.7	0.85 / 1.7
$\beta_{\rm N}^{\rm sat}$	0.9	1.5
$\beta_{\rm N}^{\rm marg}$	0.4	0.8
$W_{\rm sat}$	0.12	0.15
$W_{\rm marg}$	0.06	0.08
$d_{\rm EC}$	0.08	0.05
$(j_{\rm EC}/j_{\rm BS})_{\rm min}$	0.35–0.46	0.2–0.4
$\Delta\rho_{\rm mis}$	0.02	$\lesssim 0.01$

Table 1. Parameters for the two configurations. The values of $W_{\rm sat}$, $W_{\rm marg}$ and $d_{\rm EC}$ are normalized to the volume-averaged plasma minor radius.

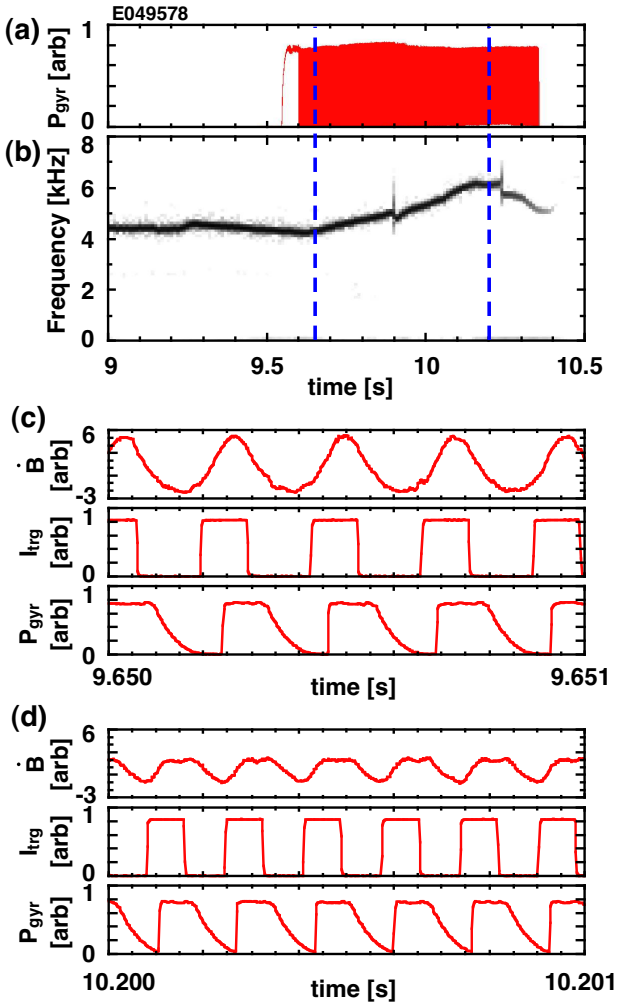

Figure 5. Typical discharge of NTM stabilization with modulated ECCD. (a) Power from gyrotron ($P_{\rm gyr}$), (b) frequency spectrum of magnetic perturbations. Magnetic probe signal ($\dot{B}$), trigger signal at the gyrotron ($I_{\rm trig}$) and power from the gyrotron at (c) t =9.65 s and (d) 10.2 s. Slow decay of the $P_{\rm gyr}$ signal at the turnoff is attributed to impedance mismatching in the signal line, and does not reflect real power; EC wave power is immediately shut down in reality.

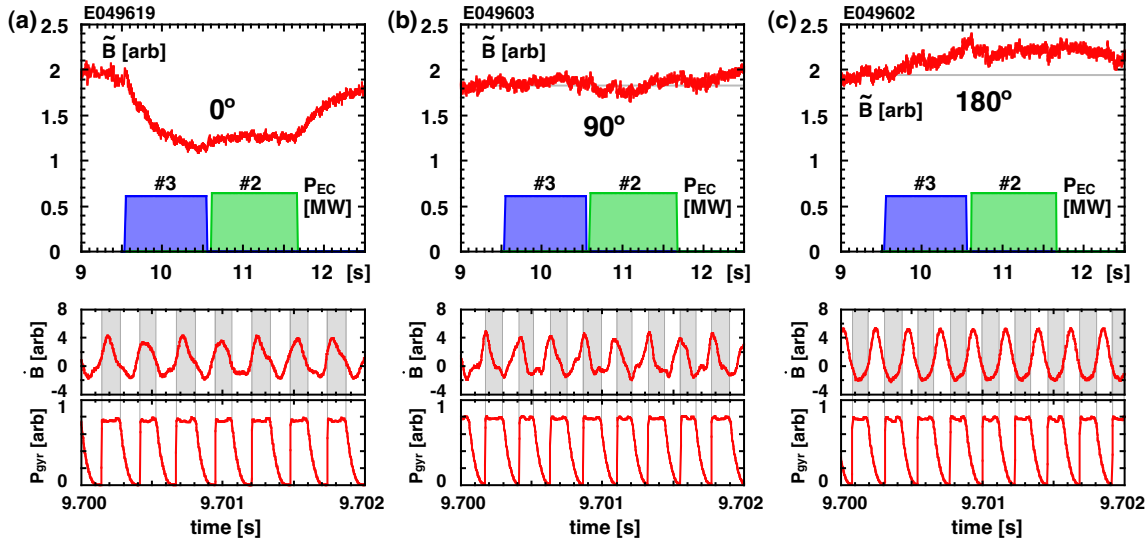

Figure 6. Temporal evolution of magnetic perturbation amplitude, EC wave power, magnetic probe signal and gyrotron power for (a) 0°, (b) 90 ° and 180° phase differences.

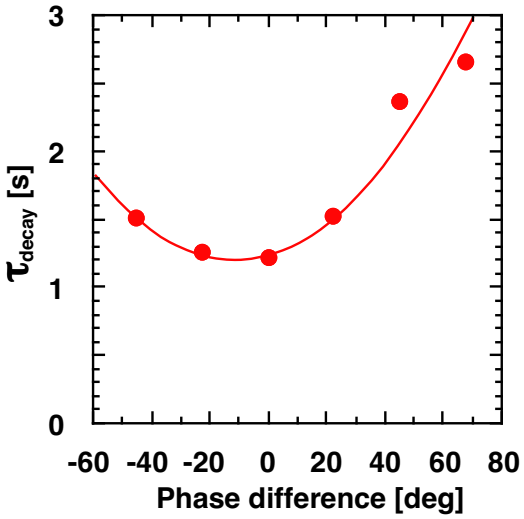

Figure 7. Dependence of decay time of magnetic perturbation amplitude on phase difference.

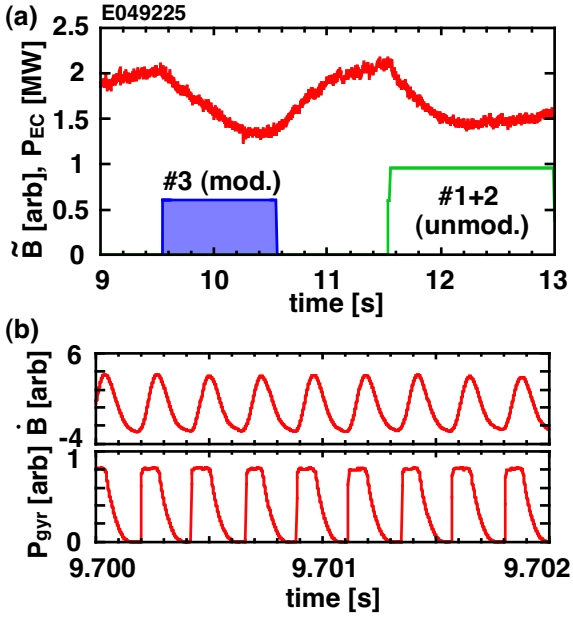

Figure 8. (a) Temporal evolution of magnetic perturbation amplitude for modulated ECCD (#3) followed by unmodulated ECCD (#1+2), (b) magnetic perturbation signal and gyrotron output power at $t = 9.7$ s.

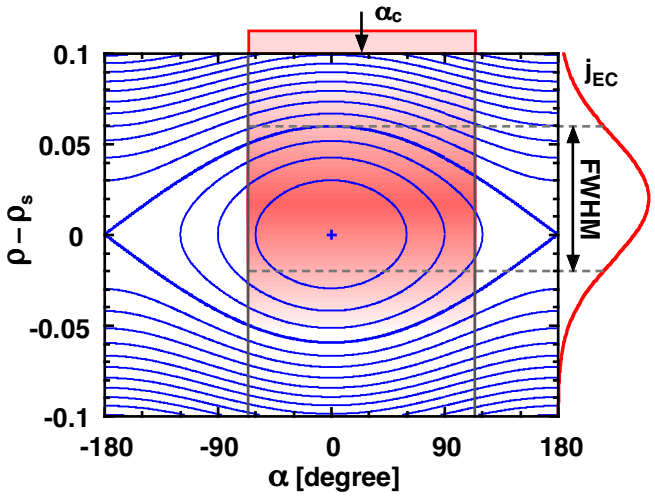

Figure 9. Schematics of island structure and ECCD profile. In this figure, full island width, FWHM of ECCD deposition width and misalignment of ECCD location are 0.12, 0.08 and 0.02, respectively. All the values are normalized to the volume-averaged plasma minor radius.

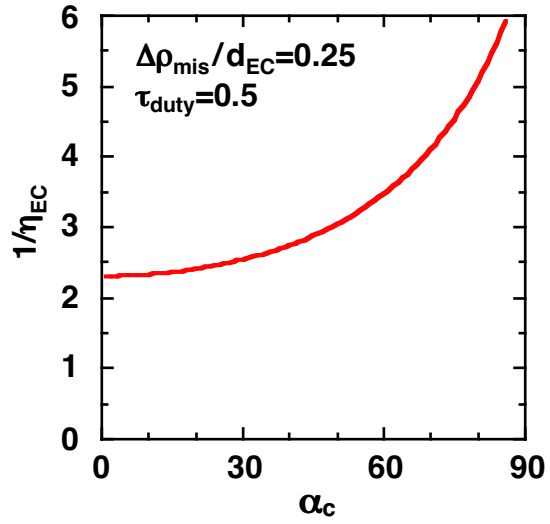

Figure 10. Dependence of the inverse of the ECCD efficiency, $1/\eta_{\rm EC}$, on the center phase of the modulation $\alpha_{\rm c}$. The values of misalignment $\Delta\rho_{\rm mis}/d_{\rm EC}$ and duty ratio $\tau_{\rm duty}$ are the ones in the JT-60U experiments.

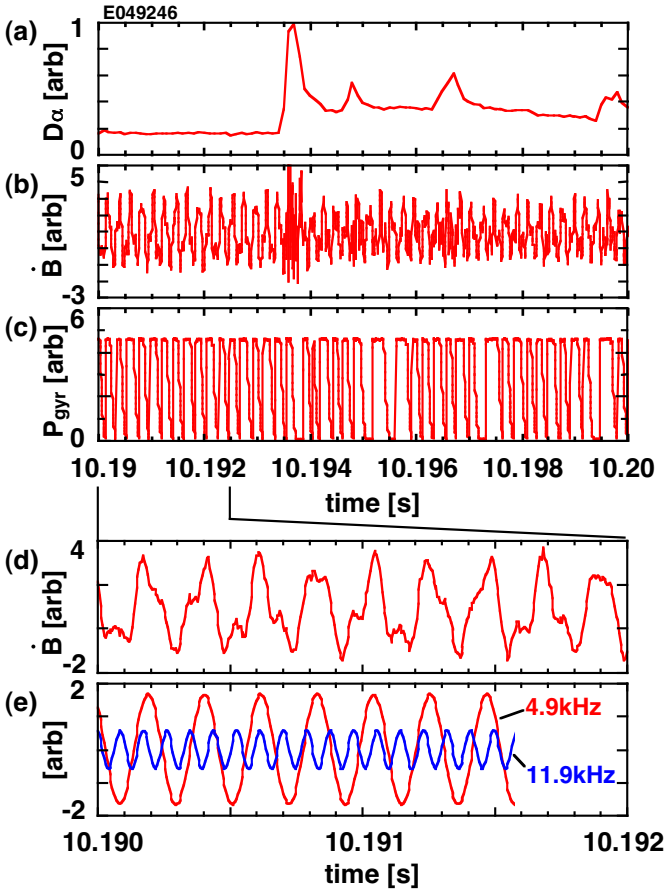

Figure 11. Time trace of (a) D_α intensity, (b) magnetic perturbations and (c) gyrotron output power. Expanded figure of (d) magnetic perturbations and (e) two major components of the perturbations obtained by Fourier transformation of the magnetic perturbation signal. The larger-amplitude signal corresponds to 2/1 NTM, while the smaller-amplitude signal corresponds to 3/2 NTM.